

irbasis: Open-source database and software for intermediate-representation basis functions of imaginary-time Green's function

Naoya Chikano^a, Kazuyoshi Yoshimi^b, Junya Otsuki^c, Hiroshi Shinaoka^a

^a*Department of Physics, Saitama University, Saitama 338-8570, Japan*

^b*Institute for Solid State Physics, University of Tokyo, Chiba 277-8581, Japan*

^c*Department of Physics, Tohoku University, Sendai 980-8578, Japan*

Abstract

The open-source library, irbasis, provides easy-to-use tools for two sets of orthogonal functions named intermediate representation (IR). The IR basis enables a compact representation of the Matsubara Green's function and efficient calculations of quantum models. The IR basis functions are defined as the solution of an integral equation whose analytical solution is not available for this moment. The library consists of a database of pre-computed high-precision numerical solutions and computational code for evaluating the functions from the database. This paper describes technical details and demonstrates how to use the library.

Keywords: Matsubara/imaginary-time Green's function, many-body quantum theories

PROGRAM SUMMARY

Program Title: irbasis

Journal Reference:

Catalogue identifier:

Licensing provisions: MIT license

Programming language: C++, Python.

Computer: PC, HPC cluster

Operating system: Any, tested on Linux and Mac OS X

RAM: less than 100 MB.

Number of processors used: 1.

Keywords: Imaginary-time Green's function, Matsubara Green's function

Classification: 4.4

External routines/libraries: numpy, scipy and h5py for Python library, HDF5 C library for C++ library.

Nature of problem: Numerical orthogonal systems for Green's function

Solution method: Galerkin method, piece-wise polynomial representation

Running time: < 1 min

1. Introduction

In condensed matter physics, Matsubara Green's function techniques are powerful tools to study many-body physics in strongly correlated systems. Examples include diagrammatic expansions such as the random phase approximation (RPA), the dynamical mean-field theory (DMFT) [1, 2], GW method [3–5]), continuous-time quantum Monte Carlo (QMC) methods [6–10].

In practical calculations, the data of the Green's function is stored in computer memory. When the Green's function is represented in the Matsubara-frequency domain as $G(i\omega_n)$, it exhibits a power-law decay at high frequencies. Thus, the number of Matsubara frequencies required for representing $G(i\omega_n)$ grows rapidly with decreasing temperature. Especially when the Green's function has other indices as spin, orbit, and wavenumber, the data of $G(i\omega_n)$ becomes huge at low temperatures. Therefore, there is a high demand for a compact representation of the imaginary-time dependence of the Green's function in practical calculations. Orthogonal polynomial representations of the Green's function are a common way to represent the data compactly [11, 12].

Recently, it was found that there is a physical complete basis set which yields a much more com-

Email address: shinaoka@mail.saitama-u.ac.jp
(Hiroshi Shinaoka)

pact representation of the Green's function [13–15] than the conventionally used classical orthogonal polynomials such as Legendre/Chebyshev polynomials. This physical representation was named the *intermediate representation* (IR). As illustrated in Fig. 1, the IR has been applied to a stable analytical continuation of QMC data to real frequencies in conjunction with sparse modeling techniques in data science [16], fast QMC sampling of the single-/two-particle Green's function [13], and the analysis of the self-energy computed by DMFT calculations with exact-diagonalization techniques [17]. The use of the IR basis functions thus will open up new and interesting research applications in condensed matter physics.

Figure 2 shows a typical example of the IR basis functions. The basis consists of a pair of two *complete* and *orthogonal* basis sets $\{u_l^\alpha(x)\}, \{v_l^\alpha(y)\}$ (x, y correspond to imaginary time and real frequency as described later). They depend on the statistics α (fermions or bosons) and a dimensionless parameter $\Lambda > 0$ (the definition is given later). They involve Legendre polynomials as a special limit of $\Lambda = 0$. The IR basis functions share favorable mathematical properties (e.g., orthogonality) with classical orthogonal polynomials. Thus, the IR basis can be used in many applications. However, *one practical problem remains to be solved as described below*.

There exist many numerical libraries for evaluating classical orthogonal polynomials. The evaluation is immediate thanks to their recurrence relations. On the other hand, the IR basis functions are the solution of an integral equation whose analytical solution is not available for the moment. For applications ranging from QMC to diagrammatic calculations, the basis functions must be determined typically within a relative error of 10^{-8} . Recently, some of the authors developed a method for computing a precise numerical solution of the integral equation [15]. To reach such precision, however, the algorithm must be implemented in arbitrary-precision arithmetic because the integral equation is ill-conditioned. This makes the computation very expensive and requires the use of a arbitrary-precision library such as GMP. Furthermore, a special care must be taken to avoid discretization errors in representing the rapidly oscillating basis functions (see Fig. 2).

Thus, there is still missing an easy-to-use and computationally cheap numerical library for evaluating the IR basis functions. Our *irbasis* library eliminates this bottleneck by providing a database

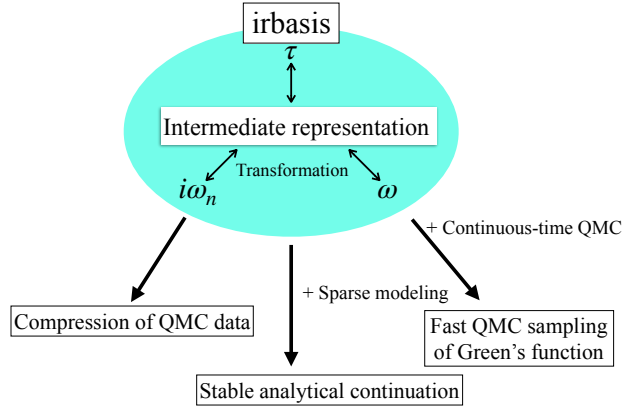


Figure 1: (Color online) Overview of the functionality of *irbasis* and applications.

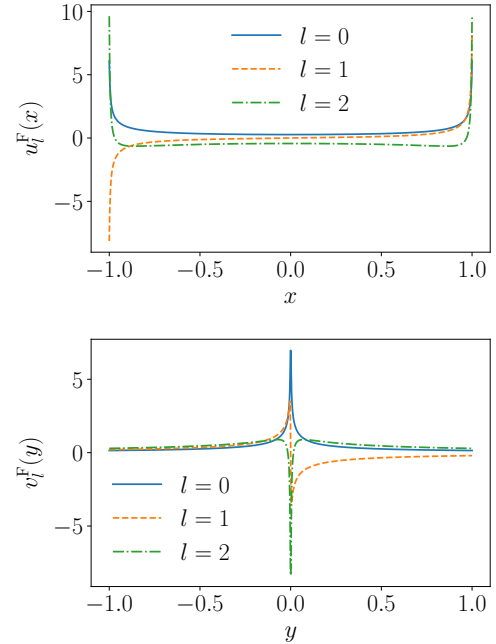


Figure 2: (Color online) IR basis functions $u_l^\alpha(x)$ and $v_l^\alpha(y)$ for $\Lambda = 1000$ and fermions. x and y are dimensionless variables corresponding to imaginary time and real frequency, and l enumerates the basis functions. These two sets of basis functions are orthonormalized with a constant weight function of 1 in $[-1, 1]$, respectively.

of pre-computed precise numerical solutions and a simple and fast tool for interpolating basis functions. The library is implemented in popular programming languages with minimal dependencies on external libraries to ensure its portability. The interpolation is performed in double-precision arithmetic but with a controlled accuracy, being computationally inexpensive. These features will enable to use IR basis functions as easily as classical orthogonal polynomials in many practical applications without technical difficulties.

The remainder of this paper is organized as follows. In Section 2, we review the definition of IR basis functions and establish notations. We describe the structure of irbasis library in Section 3. The installation and usage including examples of how to use the library are described in Sections 4 and 5, respectively. Section 6 presents a summary.

2. Intermediate representation (IR) basis function

2.1. Definition

We briefly introduce the definition of the IR basis functions following the previous studies with a slight modification of notations. We start with the spectral (Lehmann) representation of the single-particle Greens function $G^\alpha(\tau)$ in the imaginary-time domain

$$G^\alpha(\tau) = - \int_{-\omega_{\max}}^{\omega_{\max}} d\omega K^\alpha(\tau, \omega) \rho(\omega) \quad (1)$$

where β is the inverse temperature and we assume $\hbar = 1$. The superscript α specifies statistics: $\alpha = F$ for fermion and $\alpha = B$ for boson. The spectral function is defined as

$$\rho^\alpha(\omega) = -\frac{1}{\pi\omega^{\delta_{\alpha,B}}} \text{Im}G^\alpha(\omega + i0). \quad (2)$$

We assume that the spectrum $\rho^\alpha(\omega)$ is bounded in the interval $[-\omega_{\max}, \omega_{\max}]$, where ω_{\max} is a cutoff frequency. The kernel $K^\alpha(\tau, \omega)$ reads

$$K^\alpha(\tau, \omega) \equiv \omega^{\delta_{\alpha,B}} \frac{e^{-\tau\omega}}{1 \pm e^{-\beta\omega}}. \quad (3)$$

for $0 \leq \tau \leq \beta$. Here, the $+$ ($-$) sign is for fermions and bosons, respectively. The extra ω 's for boson in Eqs. (2) and (3) was introduced to avoid a singularity of the kernel at $\omega = 0$.

For given ω_{\max} and β , the IR basis functions are defined through the decomposition

$$K^\alpha(\tau, \omega) = \sum_{l=0}^{\infty} S_l^\alpha U_l^\alpha(\tau) V_l^\alpha(\omega), \quad (4)$$

where $\int_0^\beta d\tau U_l^\alpha(\tau) U_{l'}^\alpha(\tau) = \int_{-\omega_{\max}}^{\omega_{\max}} d\omega V_l^\alpha(\omega) V_{l'}^\alpha(\omega) = \delta_{ll'}$. Taking $U_l^\alpha(\beta) > 0$, we fix the sign of $U_l^\alpha(\tau)$ and $V_l^\alpha(\omega)$. This decomposition corresponds to the singular value decomposition (SVD) of the matrix representation of the kernel defined on a discrete τ - ω space. Singular values $S_l^\alpha (> 0)$ are given in decreasing order. Note that $U_l^\alpha(\tau) = (-1)^l U_l^\alpha(\beta - \tau)$ and $V_l^\alpha(\omega) = (-1)^l V_l^\alpha(-\omega)$ for $0 < \tau < \beta$. The basis functions and singular values can be computed by solving the integral equation

$$S_l^\alpha U_l^\alpha(\tau) = \int_{-\omega_{\max}}^{\omega_{\max}} d\omega K^\alpha(\tau, \omega) V_l^\alpha(\omega). \quad (5)$$

The imaginary-time Green's function and the corresponding spectral function can be expanded as

$$G^\alpha(\tau) = \sum_{l=0}^{\infty} G_l^\alpha U_l^\alpha(\tau), \quad (6)$$

$$\rho^\alpha(\omega) = \sum_{l=0}^{\infty} \rho_l^\alpha V_l^\alpha(\omega), \quad (7)$$

where

$$G_l^\alpha = -S_l^\alpha \rho_l^\alpha. \quad (8)$$

The orthogonality of basis functions yields the inverse transform of Eqs. (6) and (7) as

$$G_l^\alpha = \int_0^\beta d\tau G^\alpha(\tau) U_l^\alpha(\tau) \quad (9)$$

$$= -S_l^\alpha \int_{-\omega_{\max}}^{\omega_{\max}} d\omega \rho^\alpha(\omega) V_l^\alpha(\omega), \quad (10)$$

$$\rho_l^\alpha = \int_{-\omega_{\max}}^{\omega_{\max}} d\omega \rho^\alpha(\omega) V_l^\alpha(\omega). \quad (11)$$

Note that a constant term in $G^B(\tau)$ is not represented by the IR basis compactly, and thus should be treated separately (refer to [Appendix D](#) and Ref. [15]).

A striking feature of this decomposition is the exponential decay of S_l^α . This guarantees that G_l^α decay fast no matter how fast ρ_l^α decay.

The Matsubara-frequency representation of the Green's function can be obtained by the Fourier transformations

$$G^\alpha(i\omega_n) = \mathcal{F}(G^\alpha(\tau)) = \int_0^\beta d\tau G^\alpha(\tau) e^{i\omega_n \tau} = \sum_{l=0}^{\infty} G_l^\alpha U_l^\alpha(i\omega_n) \quad (12)$$

$$\text{with } U_l^\alpha(i\omega_n) \equiv \int_0^\beta d\tau U_l^\alpha(\tau) e^{i\omega_n \tau}, \quad (13)$$

where $U_l(i\omega_n)$ is the Fourier transformation of $U(\tau)$. \mathcal{F} is the Fourier transformation operator.

Equation (1) can be reformulated as

$$G^\alpha(i\omega_n) = \int_{-\infty}^{\infty} d\omega K^\alpha(i\omega_n, \omega) \rho^\alpha(\omega), \quad (14)$$

where

$$K^F(i\omega_n, \omega) \equiv -\mathcal{F}(K^F(\tau, \omega)) = \frac{1}{i\omega_n - \omega}, \quad (15)$$

$$K^B(i\omega_n, \omega) \equiv -\mathcal{F}(K^B(\tau, \omega)) = \frac{\omega}{i\omega_n - \omega}. \quad (16)$$

The decomposition of $K^\alpha(i\omega_n, \omega)$ reads

$$K^\alpha(i\omega_n, \omega) = - \sum_{l=0}^{\infty} S_l U_l(i\omega_n) V_l(\omega). \quad (17)$$

2.2. Dimensionless representation

In practical implementation, it is convenient to use the dimensionless form of IR basis function $u_l^\alpha(x)$ and $v_l^\alpha(y)$ proposed in Ref. [13]. The dimensionless form of the basis functions $u_l^\alpha(x)$ and $v_l^\alpha(y)$ and singular values s_l^α are defined by the decomposition

$$k^\alpha(x, y) = \sum_{l=0}^{\infty} s_l^\alpha u_l^\alpha(x) v_l^\alpha(y) \quad (18)$$

in the intervals of $x \in [-1, 1]$ and $y \in [-1, 1]$. The basis functions $u_l^\alpha(x)$ and $v_l^\alpha(y)$ are orthonormalized in these intervals, respectively. Here, the dimensionless form of the kernels is defined as

$$k^F(x, y) \equiv \frac{e^{-\frac{\Lambda}{2}xy}}{2 \cosh(\frac{\Lambda}{2}y)}, \quad (19)$$

$$k^B(x, y) \equiv y \frac{e^{-\frac{\Lambda}{2}xy}}{2 \sinh(\frac{\Lambda}{2}y)}, \quad (20)$$

where Λ is a dimensionless parameter. We take $u_l^\alpha(1) > 0$, which also fixes the sign of $v_l^\alpha(y)$. Note that $u_l^\alpha(x) = (-1)^l u_l^\alpha(x)$ and $v_l^\alpha(y) = (-1)^l v_l^\alpha(-y)$. They satisfy

$$s_l^\alpha u_l^\alpha(x) = \int_{-1}^1 dy k^\alpha(x, y) v_l^\alpha(y). \quad (21)$$

We should note that the dimensionless form of the basis functions depend on only one parameter, Λ .

Comparing Eqs. (5) and (18) establishes the relations between the two representations

$$\Lambda = \beta \omega_{\max}, \quad (22)$$

$$U_l^\alpha(\tau) = \sqrt{\frac{2}{\beta}} u_l^\alpha(x(\tau)), \quad (23)$$

$$V_l^\alpha(\omega) = \sqrt{\frac{1}{\omega_{\max}}} v_l^\alpha(y(\omega)), \quad (24)$$

$$S_l^\alpha = \sqrt{\frac{\beta \omega_{\max}^{1+2\delta_{\alpha, B}}}{2}} s_l^\alpha, \quad (25)$$

$$U_l^\alpha(i\omega_n) = \sqrt{\beta} u_{nl}^\alpha, \quad (26)$$

where $x(\tau) = 2\tau/\beta - 1 \in [-1, 1]$, $y(\omega) = \omega/\omega_{\max} \in [-1, 1]$. Here, we defined

$$u_{nl}^\alpha \equiv \frac{1}{\sqrt{2}} \int_{-1}^1 dx e^{i\pi\{n+(1/2)\delta_{\alpha, F}\}(x+1)} u_l^\alpha(x). \quad (27)$$

2.3. Solution of integral equation

One can solve the integral equation in Eq. (21) to an arbitrary precision using the procedure described in the previous study [15]. This is done by representing $u_l^\alpha(x)$ and $v_l^\alpha(y)$ as piece-wise polynomials and converting the original continuous problem to a discrete problem using the Galerkin method. We refer the interested reader to Ref. [15] for more technical details.

3. Structure of the library

The irbasis library consists of the following three files:

- `irbasis.h5` : database file in HDF5 format
- `irbasis.hpp` : C++ header file
- `irbasis.py` : Python script file

The first file, `irbasis.h5`, stores pre-computed basis functions, $u_l^\alpha(x)$ and $v_l^\alpha(y)$, and the singular values s_l^α for $\Lambda = 10, 10^2, 10^3, 10^4$. The data structure is described later. The rest two files, `irbasis.hpp` and `irbasis.py`, provide interfaces to the database for evaluating values of $u_l^\alpha(x)$ and $v_l^\alpha(y)$ in C++ and Python, respectively. The computation of other related quantities such as u_{nl}^α in Eq. (27) is also implemented.

The database has been created in the following procedure. First, we solved the integral equation (21) in arbitrary-precision arithmetic using a Python library, `irlib`, developed by some of the authors [18]. This implements the method proposed in the previous study [15]. Here, all the basis functions that satisfy $s_l^\alpha/s_0^\alpha > 10^{-12}$ are computed. In practice, $u_l^\alpha(x)$ and $v_l^\alpha(y)$ are represented as piecewise polynomials defined on multiple domains. The degree of polynomials was chosen to be 8¹. Solving the integral equation for the largest value of Λ took a couple of hours on a single CPU core of a standard laptop computer. Then, we stored the data of the piece-wise polynomial form of the basis functions and singular values in HDF5 format [19] as double precision floating numbers. The format of the database file is detailed in [Appendix A](#).

When using `irbasis.hpp` and `irbasis.py`, the basis functions are interpolated in double-precision arithmetic but with sufficient numerical accuracy. To be specific, we have confirmed that $|\Delta u_l^\alpha(x)|/\max_x |u_l^\alpha(x)|$ and $|\Delta v_l^\alpha(y)|/\max_y |v_l^\alpha(y)|$ are smaller than 10^{-8} at any x and y for all l . Here, $\Delta u_l^\alpha(x)$ and $\Delta v_l^\alpha(y)$ are the deviations of the interpolated values from the reference data evaluated by arbitrary-precision mathematic. The procedure of computing u_{nl}^α is explained in detail in [Appendix B](#).

If basis functions for any other values of Λ are required, users can make an original database by repeating the above-mentioned procedure (see the online instruction [20]).

4. Installation

The latest version of the source code, samples and the database file can be downloaded from the public repository `SpM-lab/irbasis` in GitHub [20]. The

¹ Using a smaller degree of piece-wise polynomial substantially increases the data size and the time to solution for the integral equation because more domains are required to represent the basis functions with the desired accuracy.

Python library `irbasis.py` depends a few standard packages: `numpy`, `h5py`, `future` (`future` is used to support both Python 2 and Python 3). After putting `irbasis.py` and `irbasis.h5` into the working directory, we can import `irbasis` from our Python project. It is noted that `irbasis` libraries are included in a public repository of software for the Python programming language (PyPI) [21]. Thus, if only the python library is needed, it can be easily installed by executing the following command (the `$` sign designates a shell prompt):

```
$ pip install irbasis
```

On the other hand, to use `irbasis.hpp`, the HDF5 C library [19] is required. After installing it, we can use the `irbasis` library in our C++ project just by including `irbasis.hpp`. We note that the HDF5 C library must be linked to the executable at compile time. We also provide unit tests for confirming the functionality of the `irbasis` library. They can be run via `CTest` and `CMake`. More information on the usage is found on the official wiki page for `irbasis` [20].

5. Usage

To use the `irbasis` library, we first specify the dimensionless parameter $\Lambda \equiv \beta\omega_{\max}$ and the statistics. In practical calculations, the inverse temperature β is usually given. Thus, Λ can be selected by setting the cutoff frequency ω_{\max} to a sufficiently large value such as the spectrum is bounded in $[-\omega_{\max}, \omega_{\max}]$. After setting these parameters, the data is loaded into memory from `irbasis.h5`. Then, we can interpolate basis functions and compute u_{nl}^α by calling appropriate functions as described in Section 2.2 and [Appendix A](#). In the following, we will demonstrate how to use the libraries and perform typical operations in many-body calculations such as transformation of data between the imaginary-time domain, the Matsubara-frequency domain and IR.

Some of the sample Python scripts introduced below depend on additional Python libraries (`matplotlib` and `scipy`).

5.1. Basic usage

The following pseudo code demonstrates the usage of the interface of `irbasis.py` and `irbasis.hpp`.

```

# Load basis for fermions
Lambda = 1000.0
b = load('F', Lambda, "./irbasis.h5")

# Print all singular values
for l = 0 to b.dim()-1:
    print b.s1(l)

# Evaluate basis functions
for l = 0 to b.dim()-1:
    # Any x, y in [-1, 1]
    x = 1
    y = 1

    # u_l(x) and v_l(y)
    print b.ulx(l, x)
    print b.vly(l, y)

    # k-th derivative of u_l(x) and v_l(y)
    for k = 1, 2, 3:
        print b.d_ulx(l, x, k)
        print b.d_vly(l, y, k)

# Compute u_{ln} as a matrix for given
# Matsubara frequencies
nmax = 1000
unl = b.compute_unl([0, 1, ..., nmax-1])

```

You can load pre-computed data from a HDF5 file and evaluate basis functions. We include implementations in Python (`api.py`) and C++ (`api.cpp`) in the software package.

Figure 2 shows the IR basis functions $u_l^\alpha(x)$ and $v_l^\alpha(y)$ for $\Lambda = 1000$ and $\alpha = F$. This figure was plotted by running the Python script `uv.py` included in the software package. One can see that the basis functions are even/odd functions for even/odd l .

5.2. Basis transformation

We now demonstrate how to transform the Green's function between three different representations for the imaginary-time domain $(\tau, i\omega_n, \text{IR})$. To this end, for simplicity, we consider a simple case of fermions where the imaginary-time Green's function reads

$$G(\tau) = -K^F(\tau, \epsilon) \quad (28)$$

with $\epsilon = 2$ and $\beta = 100$. The corresponding Matsubara Green's function is

$$G(i\omega_n) = \frac{1}{i\omega_n - \epsilon}. \quad (29)$$

The following procedure applies to more general cases in a straightforward fashion.

We illustrate the procedure in Fig. 3. In general, for any given $G(\tau)$, expansion coefficients G_l can

be computed by evaluating the integral in Eq. (9) numerically. This can be done very efficiently using the procedure described in [Appendix C](#).

The upper panel of Fig. 4 shows results of G_l computed by numerical integration for $\Lambda = 1000$. The lower panel of Fig. 4 compares $G(i\omega_n)$ reconstructed from G_l with the exact one in Eq. (29). We used the script file `giwn.py` in the sample directory. The expansion coefficients G_l decay exponentially as expected. We confirmed that G_l computed by numerical integral are consistent with exact results (see [Appendix D](#)) within numerical accuracy. In contrast, $G(i\omega_n)$ given in Eq. (29) decay as a power law. Note that the fast decay of G_l is guaranteed by the decay of singular value. In the lower panel of Fig. 4, we compare the exact data of $G(i\omega_n)$ and the data reconstructed from the compressed data in the IR, where one can see a perfect agreement. This demonstrates that no information is lost during the transformation between different representations in the imaginary-time domain.

Note that the transformation of the imaginary-time data to the spectral function on the real-frequency axis is an infamous ill-posed problem (*analytical continuation*). This problem can be solved by using sparse-modeling techniques in data science in conjunction with IR [16]. The implementation of the sparse-modeling analytical continuation is however beyond the scope of this software package.

6. Summary

The IR basis yields an extremely compact representation of the Matsubara Green's function. To obtain the IR basis, however, we need to solve an integral equation, which prevents the IR basis from coming into practical use in many applications. The library, `irbasis`, includes pre-computed high-precision numerical solutions. The database contains numerical solutions for typical values of the dimensional parameter Λ , which will be sufficient for most of practical applications. Nevertheless, users can add solutions for arbitrary values of Λ to the database if needed. This library allows to use the IR basis as easily as other special functions such as Legendre polynomials, open up new and interesting research applications in computations of quantum systems.

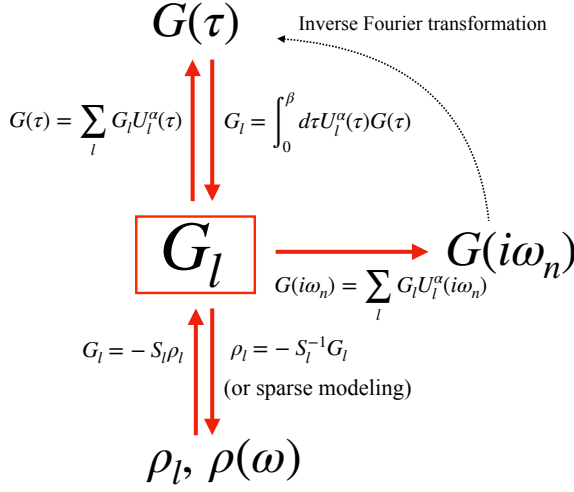


Figure 3: (Color online) Schematic of basis transformation between different representations. The red bold arrows denote the transformations supported by this software and sample programs. The sparse-modeling analytical continuation is not implemented.

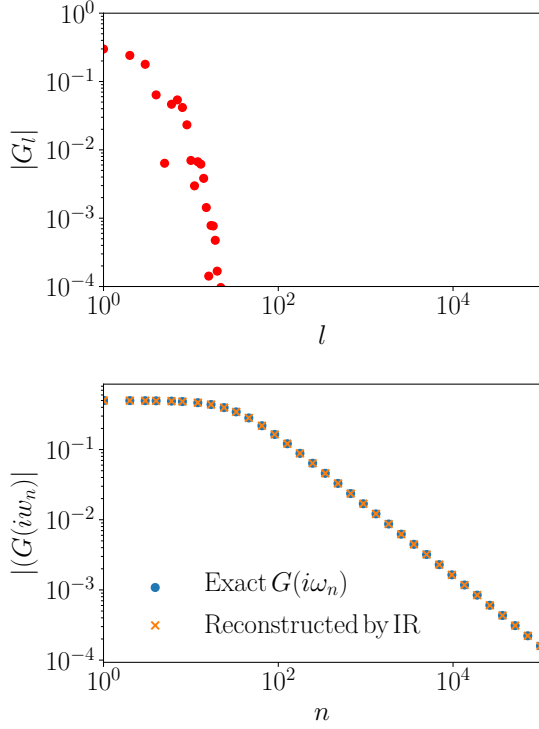


Figure 4: (Color online) Expansion coefficients in IR G_l and Matsubara-frequency data $G(i\omega_n)$.

Acknowledgments

We thank Yuki Nagai for useful feedback. HS was supported by JSPS KAKENHI Grant No. 16K17735. HS and JO were supported by JSPS KAKENHI Grant No. 18H04301 (J-Physics). HS, KY and JO were supported by JSPS KAKENHI Grant No. 18H01158. KY was supported by Building of Consortia for the Development of Human Resources in Science and Technology, MEXT, Japan.

References

References

- [1] A. Georges, G. Kotliar, W. Krauth, M. J. Rozenberg, **Dynamical mean-field theory of strongly correlated fermion systems and the limit of infinite dimensions**, *Reviews of Modern Physics* 68 (1) (1996) 13–125. [doi:10.1103/RevModPhys.68.13](https://doi.org/10.1103/RevModPhys.68.13). URL http://adsabs.harvard.edu/cgi-bin/nph-data_query?bibcode=1996RvMP...68...13G&link_type=EJOURNAL
- [2] J. M. Tomczak, M. Casula, T. Miyake, F. Aryasetiawan, S. Biermann, **Combined gw and dynamical mean-field theory: Dynamical screening effects in transition metal oxides**, *EPL (Europhysics Letters)* 100 (6) (2012) 67001. URL <http://stacks.iop.org/0295-5075/100/i=6/a=67001>
- [3] L. Hedin, **New method for calculating the one-particle Green's function with application to the electron-gas problem**, *Physical Review* 139 (3A) (1965) A796.
- [4] M. J. van Setten, F. Weigend, F. Evers, **The gw-method for quantum chemistry applications: Theory and implementation**, *Journal of Chemical Theory and Computation* 9 (1) (2013) 232–246, PMID: 26589026. [arXiv:https://doi.org/10.1021/ct300648t](https://arxiv.org/abs/https://doi.org/10.1021/ct300648t), [doi:10.1021/ct300648t](https://doi.org/10.1021/ct300648t). URL <https://doi.org/10.1021/ct300648t>
- [5] F. Aryasetiawan, O. Gunnarsson, **The gw method**, *Reports on Progress in Physics* 61 (3) (1998) 237. URL <http://stacks.iop.org/0034-4885/61/i=3/a=002>
- [6] A. Rubtsov, V. Savkin, A. Lichtenstein, **Continuous-time quantum Monte Carlo method for fermions**, *Physical Review B* 72 (3) (2005) 035122. [doi:10.1103/PhysRevB.72.035122](https://doi.org/10.1103/PhysRevB.72.035122). URL <http://link.aps.org/doi/10.1103/PhysRevB.72.035122>
- [7] P. Werner, A. Comanac, L. de' Medici, M. Troyer, A. Millis, **Continuous-Time Solver for Quantum Impurity Models**, *Physical Review Letters* 97 (7) (2006) 076405. [doi:10.1103/PhysRevLett.97.076405](https://doi.org/10.1103/PhysRevLett.97.076405). URL <http://link.aps.org/doi/10.1103/PhysRevLett.97.076405>
- [8] E. Gull, P. Werner, O. Parcollet, M. Troyer, **Continuous-time auxiliary-field Monte Carlo for quantum impurity models**, *EPL (Europhysics Letters)* 82 (5) (2008) 57003. [doi:10.1209/0295-5075/82/57003](https://doi.org/10.1209/0295-5075/82/57003). URL <http://stacks.iop.org/0295-5075/82/i=5/a=57003?key=crossref>. <https://doi.org/10.1209/0295-5075/82/57003>

- [9] J. Otsuki, H. Kusunose, P. Werner, Y. Kuramoto, **Continuous-Time Quantum Monte Carlo Method for the Coqblin-Schrieffer Model**, Journal of the Physical Society of Japan 76 (11) (2007) 114707–11. [doi:10.1143/JPSJ.76.114707](https://doi.org/10.1143/JPSJ.76.114707). URL <http://journals.jps.jp/doi/10.1143/JPSJ.76.114707>
- [10] E. Gull, A. J. Millis, A. I. Lichtenstein, A. N. Rubtsov, M. Troyer, P. Werner, **Continuous-time Monte Carlo methods for quantum impurity models**, Reviews of Modern Physics 83 (2) (2011) 349–404. [doi:10.1103/RevModPhys.83.349](https://doi.org/10.1103/RevModPhys.83.349). URL <http://link.aps.org/doi/10.1103/RevModPhys.83.349>
- [11] L. Boehnke, H. Hafermann, M. Ferrero, F. Lechermann, O. Parcollet, Orthogonal polynomial representation of imaginary-time Green's functions, Physical Review B - Condensed Matter and Materials Physics 84 (7) (2011) 1–13. [arXiv:1104.3215](https://arxiv.org/abs/1104.3215), [doi:10.1103/PhysRevB.84.075145](https://doi.org/10.1103/PhysRevB.84.075145).
- [12] E. Gull, S. Iskakov, I. Krivenko, A. A. Rusakov, D. Zgid, **Chebyhsev polynomial representation of imaginary time response functions** (2018) 1–11[arXiv:1805.03521](https://arxiv.org/abs/1805.03521). URL <http://arxiv.org/abs/1805.03521>
- [13] H. Shinaoka, J. Otsuki, M. Ohzeki, K. Yoshimi, Compressing Green's function using intermediate representation between imaginary-time and real-frequency domains, Physical Review B 96 (3) (2017) 1–8. [arXiv:1702.03054](https://arxiv.org/abs/1702.03054), [doi:10.1103/PhysRevB.96.035147](https://doi.org/10.1103/PhysRevB.96.035147).
- [14] H. Shinaoka, J. Otsuki, K. Haule, M. Wallerberger, E. Gull, K. Yoshimi, M. Ohzeki, Overcomplete compact representation of two-particle Green's functions, Physical Review B 97 (20) (2018) 1–14. [arXiv:1803.01916](https://arxiv.org/abs/1803.01916), [doi:10.1103/PhysRevB.97.205111](https://doi.org/10.1103/PhysRevB.97.205111).
- [15] N. Chikano, J. Otsuki, H. Shinaoka, **Performance analysis of a physically constructed orthogonal representation of imaginary-time green's function**, Phys. Rev. B 98 (2018) 035104. [doi:10.1103/PhysRevB.98.035104](https://doi.org/10.1103/PhysRevB.98.035104). URL [https://link.aps.org/doi/10.1103/PhysRevB.98.035104](http://link.aps.org/doi/10.1103/PhysRevB.98.035104)
- [16] J. Otsuki, M. Ohzeki, H. Shinaoka, K. Yoshimi, **Sparse modeling approach to analytical continuation of imaginary-time quantum Monte Carlo data**, Physical Review E 95 (6) (2017) 061302(R)–6. [doi:10.1103/PhysRevE.95.061302](https://doi.org/10.1103/PhysRevE.95.061302). URL <http://link.aps.org/doi/10.1103/PhysRevE.95.061302>
- [17] Y. Nagai, H. Shinaoka, **Converged spectrum in the exact-diagonalization-based dynamical mean-field theory : Sparse modeling analysis with the intermediate representation** (5) (2018) 5–10. [arXiv:\protect\vrulwidth0pt\protect\href{https://arxiv.org/abs/1806.10316}{\arXiv:1806.10316}](https://arxiv.org/abs/1806.10316).
- [18] <https://github.com/SpM-lab/irlib>.
- [19] <http://www.hdfgroup.org/HDF5>.
- [20] <https://github.com/SpM-lab/irbasis>.
- [21] <https://pypi.org/project/irbasis>.

Appendix A. Format of datafile

In a database file, we store $u_l^\alpha(x)$ and $v_l^\alpha(y)$ as piece-wise polynomial defined in the interval $[0, 1]$ since these functions are even or odd. A piece-wise

polynomial $f(x)$ on $[0, 1]$ is represented in the form

$$f(x) = \sum_{s=0}^{N_s-1} \sum_{k=0}^{N_p-1} W(x, x_s, x_{s+1}) f_{sk}(x - x_s)^k, \quad (\text{A.1})$$

where f_{sk} is a coefficient of this piece-wise polynomial. N_s is a total number of points where $f(x \in [0, 1]) = 0$. The set $\{x_0 (= 0), x_1, \dots, x_{N_s} (= 1)\}$ is ascending order and $f(x)$ is equal to be 0 at each points. Here, N_p is the degree of the piece-wise polynomial and $W(x, a, b)$ is the window function defined as

$$W(x, a, b) \equiv \begin{cases} 1 & a \leq x < b, \\ 0 & \text{otherwise.} \end{cases} \quad (\text{A.2})$$

Equation (A.1) is evaluated at $x = 1$ as $f(1) = f(1 + 0^-)$. We use Eq. (A.1) to evaluate the values of IR basis functions for arbitrary values of x and y . Derivatives of the basis functions are evaluated by differentiating Eq. (A.1).

The file format of the database used in `irbasis` is HDF5. IR basis sets for different parameter sets are stored in different HDF5 groups. Each group must have the structure given in Table A.1.

Appendix B. Fourier transformation

Equation (27) is evaluated by means of numerical integration over x or a high-frequency expansion for low and high frequencies, respectively.

The high frequency expansion of u_{nl}^α is given as

$$u_{nl}^F = \sum_{m=0}^{N_P-1} \left[\frac{-1}{i\pi(n+1/2)} \right]^{m+1} \frac{u_l^{(m),F}(1) + u_l^{(m),F}(-1)}{\sqrt{2}}, \quad (\text{B.1})$$

$$u_{nl}^B = \sum_{m=0}^{N_P-1} \left[\frac{1}{i\pi(n+1)} \right]^{m+1} \frac{u_l^{(m),B}(1) - u_l^{(m),B}(-1)}{\sqrt{2}}, \quad (\text{B.2})$$

where $u_l^{(m),\alpha}(x)$ is the m -th derivative function of $u_l^\alpha(x)$. The evaluation of these equations for high frequencies is efficient and stable as long as the expansion is well converged with respect to m .

At low frequencies, we evaluate Eq. (27) by means of numerical integration for each segment (domain) of the piece-wise polynomials as

$$u_{nl}^\alpha = \frac{1}{\sqrt{2}} e^{i\Omega_n^\alpha} \sum_{s=0}^{N_s-1} J_0(x_s, x_{s+1}, \Omega_n^\alpha). \quad (\text{B.3})$$

Dataset	Type and dimensions	Description
info/Lambda	<i>double</i>	Dimensionless parameter Λ .
info/dim	<i>int</i>	Number of basis functions and singular values (<i>dim</i>).
info/statistics	<i>int</i>	Statistics (1 for fermions and 0 for bosons).
sl	<i>double (dim)</i>	Singular values s_l^α .
ulx/np	<i>int</i>	Degree of the piece-wise polynomials for $u_l^\alpha(x)$ ($= N_p^u$).
ulx/ns	<i>int</i>	Number of sections for $x \in [0, 1]$ ($= N_s^u$).
ulx/data	<i>double (dim, N_s^u, N_p^u)</i>	Coefficients of the piece-wise polynomials for $u_l^\alpha(x)$.
vly/np	<i>int</i>	Degree of the piece-wise polynomials for $v_l^\alpha(y)$ ($= N_p^v$).
vly/ns	<i>int</i>	Number of sections for $y \in [0, 1]$ ($= N_s^v$).
vly/data	<i>double (dim, N_s^v, N_p^v)</i>	Coefficients of the piece-wise polynomials for $v_l^\alpha(y)$.

Table A.1: The structure of HDF5 group for storing data of an IR basis set. The actual data types are H5T_IEEE_F64LE and H5T_STD_I64LE for *double* and *int*, respectively.

where $\Omega_n^\alpha = \pi(n + (1/2)\delta_{\alpha,F})$, N_s is the number of segments of the piece-wise polynomials for $u_l^\alpha(x)$. The end points of segments are denoted by x_s ($x_s < x_{s+1}$). To simplify the equation, we also define

$$J_k(x_s, x_{s+1}, \Omega) \equiv \int_{x_s}^{x_{s+1}} dx e^{i\Omega x} u^{(k),\alpha}(x). \quad (\text{B.4})$$

Each term is evaluated using either of the two different methods described below. For $\Omega_n^\alpha(x_{s+1} - x_s) < c\pi$ (c is a constant of $O(1)$), Equation (B.4) is evaluated precisely by means of numerical integration using a high-order Gauss Legendre quadrature formula. For $\Omega_n^\alpha(x_{s+1} - x_s) > c\pi$, we use the following recursion relation

$$J_k(x_s, x_{s+1}, \Omega) = \frac{1}{i\Omega} [e^{i\Omega x_{s+1}} f^{(k)}(x_{s+1}) - e^{i\Omega x_s} f^{(k)}(x_s) - J_{k+1}(x_s, x_{s+1}, \Omega)] \quad (\text{B.5})$$

with $J_{N_P}(x_s, x_{s+1}, \Omega) = 0$.

There are several useful relations between the matrix elements of u_{nl}^α :

$$\sum_{n \in Z} u_{nl}^* u_{nl'} = \delta_{ll'}, \quad (\text{B.6})$$

$$(u_{nl}^F)^* = u_{-n-1,l}^F = (-1)^{l+1} u_{nl}^F, \quad (\text{B.7})$$

$$(u_{nl}^B)^* = u_{-n,l}^B = (-1)^l u_{nl}^B. \quad (\text{B.8})$$

Appendix C. Computing expansion coefficients using numerical integration

For given $G(\tau)$, the expansion coefficients in terms of IR G_l can be computed by means of nu-

merical integration as

$$G_l = \int_0^\beta d\tau G(\tau) U_l^F(\tau) \quad (\text{C.1})$$

$$= \sqrt{\frac{\beta}{2}} \int_{-1}^1 dx G(\beta(x+1)/2) U_l^F(x) \quad (\text{C.2})$$

$$= \sqrt{\frac{\beta}{2}} \int_{-1}^1 dx G(\beta(x+1)/2) u_l^F(x). \quad (\text{C.3})$$

Here, the integrand functions $G(\beta(x+1)/2) u_l^F(x)$ are rapidly oscillating functions around $x = \pm 1$. These integrals can be evaluated precisely by means of composite Gauss-Legendre quadrature as detailed below.

Let us first introduce Gauss-Legendre quadrature. An n -point Gauss-Legendre quadrature rule reads

$$\int_{-1}^1 dx f(x) \simeq \sum_{i=1}^N w_i^{\text{GL}} f(x_i^{\text{GL}}), \quad (\text{C.4})$$

where the sampling points x_i^{GL} are the roots (zeros) of the N -th Legendre polynomial $P_N(x)$. The weights w_i^{GL} are $w_i^{\text{GL}} = 2/[(1 - (x_i^{\text{GL}})^2)(P'_N(x_i^{\text{GL}}))^2]$. The approximate equality becomes exact if the integrand function $f(x)$ is a polynomial of degree $2N - 1$ or less. Equation (C.4) still produces a good estimate if $f(x)$ is approximated by a polynomial of degree $2N - 1$. In practice, N is increased until convergence is reached. The computation of the sampling points and weights are implemented in many numerical libraries such as `numpy`, `GSL`, `QUADPACK`.

In the present case, the basis functions $u_l^F(x)$ are approximated well by piece-wise polynomials of

fixed degree in each section of the piece-wise polynomials. Thus, Equation (C.3) is approximated accurately

$$G_l = \sqrt{\frac{\beta}{2}} \sum_{s=0}^{N_s-1} \sum_{i=1}^N \left(\frac{x_{s+1} - x_s}{2} w_i^{\text{GL}} \right) \times G(\beta(x_{s,i} + 1)/2) u_l^{\text{F}}(x_{s,i}) \quad (\text{C.5})$$

$$= \sqrt{\frac{\beta}{2}} \sum_{j=1}^{N_s N} \tilde{w}_j G(\beta(x_j + 1)/2) u_l^{\text{F}}(x_j), \quad (\text{C.6})$$

where $x_{s,i} \equiv (x_{s+1} - x_s)(x_i^{\text{GL}} + 1)/2 + x_s$. For simplicity of presentation, we introduced $j \equiv (s, i)$ and defined the sampling points x_j and the weights $\tilde{w}_j \equiv (x_{s+1} - x_s)w_i^{\text{GL}}/2$ of the *composite* Gauss-Legendre quadrature.

In practice, this integral can be computed efficiently by a matrix multiplication as

$$G_l = \sqrt{\frac{\beta}{2}} (\mathbf{G} \mathbf{u})_{1,l}, \quad (\text{C.7})$$

where \mathbf{G} and \mathbf{u} are matrices of size $(1, nN_s)$ and (nN_s, N_l) defined as

$$\mathbf{G}_{1,i} = G(\beta(\tilde{x}_i + 1)/2), \quad (\text{C.8})$$

$$\mathbf{u}_{i,l} = \tilde{w}_i u_l^{\text{F}}(\tilde{x}_i), \quad (\text{C.9})$$

respectively. The computational complexity is $O(nN_s N_l)$. For $\Lambda = 10^4$ and $\alpha = \text{F}$ ($N_s = 134$ and $N_l = 61$), the use of $n = 16$ produces converged results.

Appendix D. IR of the Green's function with a single pole

We consider the Green's function with a single pole at ϵ :

$$G^\alpha(i\omega_n) = \frac{1}{i\omega_n - \epsilon}. \quad (\text{D.1})$$

From Eq. (17), we obtain

$$G^{\text{F}}(i\omega_n) = - \sum_{l=0}^{\infty} S_l^{\text{F}} U_l^{\text{F}}(i\omega_n) V_l^{\text{F}}(\epsilon), \quad (\text{D.2})$$

$$G^{\text{B}}(i\omega_n) = - \sum_{l=0}^{\infty} S_l^{\text{B}} U_l^{\text{B}}(i\omega_n) V_l^{\text{B}}(\epsilon) \epsilon^{-1} \quad (\text{D.3})$$

for $\alpha = \text{F}$ and B , respectively. Comparing these two equations with Eq. (12), we obtain the expansion

coefficients of the Green's function in terms of IR as

$$G_l^{\text{F}} = -S_l^{\text{F}} V_l^{\text{F}}(\epsilon), \quad (\text{D.4})$$

$$G_l^{\text{B}} = -S_l^{\text{B}} V_l^{\text{B}}(\epsilon) \epsilon^{-1}. \quad (\text{D.5})$$

In the case of $\epsilon = 0$ for bosons, the inverse transformation of $G^{\text{B}}(i\omega_n) = 1/i\omega_n$ yields $G^{\text{B}}(\tau) = -1$. Such constant terms in the τ domain are not represented compactly in the IR basis for bosons and should be treated separately. Please refer to Ref. [15] for a more detailed discussion.